Application of Turbulence Model Equations to Axisymmetric Wakes

W. S. LEWELLEN,* M. TESKE,† AND COLEMAN DUP. DONALDSON‡
Aeronautical Research Associates of Princeton, Inc., Princeton, N.J.

The second-order invariant modeling technique for turbulent flows as developed by Donaldson is applied to axisymmetric wakes. All empirical model parameters are chosen from data on jets and shear layers leaving the wake completely determined as a function of initial conditions. Model predictions for the mean velocity distribution and the distributions of the four components of the second-order stress tensor are verified by comparison with the experimental observations of Chevray for a wake with significant mean momentum and Naudascher for the wake behind a self-propelled body.

Nomenclature

a, b = model constants defined in Eq. (12)
D = diameter of the generating body
M = normalized momentum defect in the wake, see Eq. (15)
p = pressure
q = square root of twice the turbulent kinetic energy per unit mass
r = radial coordinate
r^* = radius at which $\langle w'w' \rangle^{1/2}$ reaches one half its maximum value
$r_{1/2}$ = radius at which $|\bar{w} - U_o|/w_D = \frac{1}{2}$
$\hat{r}$ = radius at which q reaches one half its maximum value
Re = Reynolds number
t = time
u = radial velocity component
u_i, u_j, u_k = Cartesian velocity components
U_o = freestream uniform velocity
v = tangential velocity component
w = axial velocity component
w_D = maximum value of $|\bar{w} - U_o|$ at any axial station
x_i, x_j, x_k = Cartesian coordinates
z = axial coordinate in the freestream direction
λ = microscale of turbulent dissipation
Λ = macroscale of turbulent model
Λ_2 = diffusion scale for third-order velocity correlations
Λ_3 = diffusion scale for pressure-velocity correlations
ν = kinematic viscosity
ρ = density
Ψ = stream function defined in Eq. (5)

Superscripts
$\bar{}$ = denotes time average
$'$ = denotes fluctuation about the mean value

Subscript
m = denotes maximum value

Introduction

As the initial step in a program to calculate the development of a turbulent wake behind a submarine, a computer model has been developed for axisymmetric wakes in a homogeneous medium. Wakes with near zero net mean momentum are examined to explore the distinction between a "momentumless wake" as exemplified by the data of Naudascher[1] and a wake with significant mean momentum as investigated experimentally by Chevray.[2]

Several variations of transport equations for the Reynolds stresses are currently being explored (see reviews by Bradshaw[3] and Mellor and Herring[4]). We will follow the method of second-order closure discussed in detail by Donaldson.[5,6] Our intent is to model the higher-order correlation terms in the simplest possible way consistent with tensor invariance and critical empirical data. The modeled terms in the transport equations contain three parameters which are determined empirically from boundary-layer and axisymmetric, freejet data. Wake calculations are made by matching the distribution of velocity, $\bar{w}$, and Reynolds stresses, $\langle u'w' \rangle$, $\langle v'v' \rangle$, $\langle u'u' \rangle$, and $\langle w'w' \rangle$ at one axial station with the data of either Chevray or Naudascher and then comparing the program predictions for the subsequent wake development with the observed development.

Description of Computer Model

The mean flow equations of motion for an incompressible fluid may be written as

$$\partial \bar{u}_j / \partial x_j = 0 \tag{1}$$

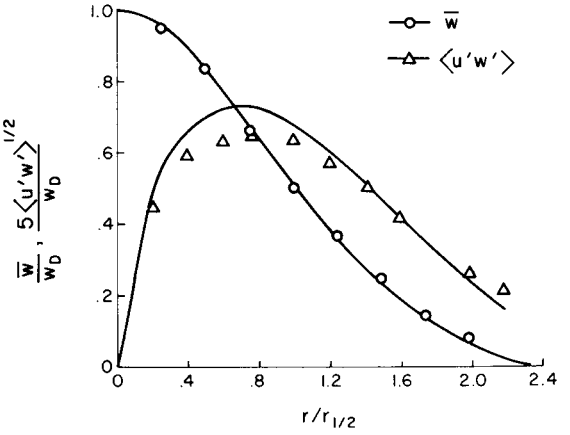

Fig. 1 Normalized mean velocity distribution and shear stress distribution of a freejet as a function of radius normalized by the radius at which $w/w_D = \frac{1}{2}$. ○ data of Wygnanski and Fiedler; —— model results for $b = 0.125$, $\Lambda = 0.2\hat{r}$, and $\Lambda_2/\Lambda = 0.3$.

Received July 5, 1973; presented as Paper 73-648 at the AIAA 6th Fluid and Plasma Dynamics Conference, Palm Springs, Calif., July 16–18, 1973; revision received November 12, 1973. This research was supported by ARPA and monitored by ONR under Contract N00014-72-C-0413.

Index categories: Jets, Wakes, and Viscid-Inviscid Flow Interactions; Subsonic and Transonic Flow; Viscous Nonboundary-Layer Flows.

* Senior Consultant. Member AIAA.
† Senior Staff.
‡ President and Senior Consultant. Associate Fellow AIAA.

$$\frac{D\bar{u}_i}{Dt} = -\frac{1}{\rho}\frac{\partial p}{\partial x_i} + \frac{\partial}{\partial x_j}\left(\nu\frac{\partial \bar{u}_i}{\partial x_j} - \langle u_i' u_j'\rangle\right) \tag{2}$$

$$\frac{D\langle u_i' u_j'\rangle}{Dt} = -\langle u_i' u_k'\rangle\frac{\partial \bar{u}_j}{\partial x_k} - \langle u_j' u_k'\rangle\frac{\partial \bar{u}_i}{\partial x_k} - \frac{\partial}{\partial x_k}\langle u_k' u_i' u_j'\rangle - \frac{1}{\rho}\frac{\partial\langle p' u_i'\rangle}{\partial x_j} - \frac{1}{\rho}\frac{\partial\langle p' u_j'\rangle}{\partial x_i} + \left\langle\frac{p'}{\rho}\left(\frac{\partial u_i'}{\partial x_j} + \frac{\partial u_j'}{\partial x_i}\right)\right\rangle + \nu\frac{\partial^2\langle u_i' u_j'\rangle}{\partial x_k^2} - 2\nu\left\langle\frac{\partial u_i'}{\partial x_k}\frac{\partial u_j'}{\partial x_k}\right\rangle \tag{3}$$

This becomes a closed set of equations when the terms involving the triple velocity fluctuation correlations, the pressure fluctuation correlations, and the correlation of the gradients of the velocity fluctuations are somehow determined in terms of the other variables.

Following the method of second-order closure, discussed in detail by Donaldson,[5,6] we can write Eq. (3) as

$$\frac{D}{Dt}\langle u_i' u_j'\rangle = -\langle u_i' u_k'\rangle\frac{\partial \bar{u}_j}{\partial x_k} - \langle u_j' u_k'\rangle\frac{\partial \bar{u}_i}{\partial x_k} + \frac{\partial}{\partial x_k}\left[q\Lambda_2\left(\frac{\partial\langle u_i' u_k'\rangle}{\partial x_j} + \frac{\partial\langle u_k' u_j'\rangle}{\partial x_i} + \frac{\partial\langle u_i' u_j'\rangle}{\partial x_k}\right)\right] + \frac{\partial}{\partial x_j}\left(q\Lambda_3\frac{\partial\langle u_i' u_k'\rangle}{\partial x_k}\right) + \frac{\partial}{\partial x_i}\left(q\Lambda_3\frac{\partial\langle u_j' u_k'\rangle}{\partial x_k}\right) - \frac{q}{\Lambda}\left(\langle u_i' u_j'\rangle - \frac{\delta_{ij}}{3}q^2\right) - 2\nu\left[\delta_{ij}\frac{q^2}{3\lambda^2} + \frac{a}{\Lambda^2}\left(\langle u_i' u_j'\rangle - \frac{\delta_{ij}q^2}{3}\right)\right] + \nu\frac{\partial^2\langle u_i' u_j'\rangle}{\partial x_k^2} \tag{4}$$

with $q^2 = \langle u_i' u_i'\rangle$, and Λ, Λ_2, Λ_3, and λ model scales to be determined. The model for the dissipation terms used is somewhat different from that in Ref. 6 in that the principle dissipation occurring on the microscale level is taken to be isotropic.

For cylindrical coordinates (r, Φ, z) with axisymmetric velocities (u, v, w), Eq. (1) may be eliminated by defining a stream function as

$$\bar{w} = (1/r)(\partial\Psi/\partial r), \qquad \bar{u} = -(1/r)(\partial\Psi/\partial z) \tag{5}$$

For the usual constant pressure wake, the pressure gradient in Eq. (2) disappears. For a thin wake it is also valid to assume $\partial/\partial z \ll \partial/\partial r$. Under these conditions the von Mises transformation may be applied to use the stream function Ψ as the primary independent variable instead of the radius; the momentum equation for a steady wake then reduces to the following scalar equation

$$\frac{\partial \bar{w}}{\partial z} = \frac{\partial}{\partial\Psi}\left[vr^2\bar{w}\frac{\partial \bar{w}}{\partial\Psi} - r\langle u'w'\rangle\right] \tag{6}$$

with

$$r^2 = 2\int_0^r \frac{d\Psi}{\bar{w}} \tag{7}$$

We are not restricted to linearized departures from the freestream velocity U_o.

The four nonzero Reynolds stress equations, when transformed from Eq. (4) lead to

$$\langle u'u'\rangle_z = [r^2\bar{w}N_{321}\langle u'u'\rangle_\Psi]_\Psi - N_{220}\langle v'v'\rangle_\Psi + (\langle v'v'\rangle - \langle u'u'\rangle)[(N_{422}/r^2\bar{w}) - (N_{020})_\Psi] - A\langle u'u'\rangle - Bq^2 \tag{8}$$

$$\langle v'v'\rangle_z = [r^2\bar{w}N_{101}\langle v'v'\rangle_\Psi]_\Psi + N_{220}\langle u'u'\rangle_\Psi + (\langle u'u'\rangle - \langle v'v'\rangle)[(N_{422}/r^2\bar{w}) + (N_{200})_\Psi] - A\langle v'v'\rangle - Bq^2 \tag{9}$$

$$\langle w'w'\rangle_z = [r^2\bar{w}N_{101}\langle w'w'\rangle_\Psi]_\Psi - 2\langle u'w'\rangle r\bar{w}_\Psi - A\langle w'w'\rangle - Bq^2 \tag{10}$$

$$(\langle u'w'\rangle/r)_z = [r^2\bar{w}N_{211}(\langle u'w'\rangle/r)_\Psi]_\Psi + N_{422}(\langle u'w'\rangle/r)_\Psi + (N_{220})_\Psi(\langle u'w'\rangle/r) - \langle u'u'\rangle\bar{w}_\Psi - A\langle u'w'\rangle/r \tag{11}$$

with

$$N_{ijk} = i\Lambda_2 q + j\Lambda_3 q + kv$$
$$A = (q + 2va/\Lambda)/\Lambda\bar{w}$$

and

$$B = (2v/3\bar{w}\lambda^2) - A/3$$

For boundary conditions, we assume that the five variables $\bar{w}$, $\langle u'w'\rangle/r$, $\langle u'u'\rangle$, $\langle v'v'\rangle$, and $\langle w'w'\rangle$ have zero slopes at $r = 0$ and all have zero values as $r \to \infty$ except $\bar{w}$ which approaches U_o.

Equations (6, 8–11) are replaced by implicit, finite-difference equations forward-facing in the z direction and centered in Ψ. We represent the Ψ derivatives at a point by fitting a quadratic through the point and its two neighbors, so that unequal Ψ spacing is permitted. Analytic expansion in r^2 about the centerline permits us to write the centerline implicit values in terms of the implicit values at the first Ψ position off $\Psi = 0$. The linearized equations are then solved by the general tridiagonal algorithm. The nonlinear terms such as $-\langle u'u'\rangle\bar{w}_\Psi$ in Eq. (11) are evaluated by giving the energy components their present step value. This assumption allows us to solve Eqs. (6) and (11) as a pair at the next step, and subsequently solve for the three energy components by Eqs. (8–10) at the next step. Since $\bar{w}$ is unknown at the next downstream position and appears on the right side of Eqs. (6) and (11) in a nonlinear role, we iterate Eqs. (6) and (11) until the maximum difference in $\bar{w}$ at the next step is less than 0.1% of its maximum value there. A typical run time on a Digital Scientific Corp. META-4 is 12 min; comparable times on an Univac 1108 and CDC 6600 are 2 min and 1 min, respectively.

Determination of Model Parameters

The model parameters λ, Λ, Λ_2, and Λ_3 must be determined to completely specify the flow problem. The hypothesis is that the same relationships between the model lengths and the characteristic flow lengths, which are empirically found to give good results for axisymmetric jets and wall shear layers, will be sufficiently valid for wake flows also.

The microscale λ is taken as

$$\lambda = \Lambda/(a + bq\Lambda/v)^{1/2} \tag{12}$$

with a and b taken to be 2.5 and 0.125, respectively. The results presented herein are relatively insensitive to the choice of a, since the Reynolds number $q\Lambda/v$ of the turbulence is always large in the calculation regions which may be checked by experiment. The choice of b is dictated by the requirement that the model *also* apply to a wall shear layer where $\langle u'w'\rangle = \text{const}$. For this special flow it is possible to show that

$$b = \langle u'w'\rangle^2/q^2\langle w'w'\rangle \tag{13}$$

Experimentally,[7] $q^2/\langle u'w'\rangle$ has a value of ≈ 7, and $\langle w'w'\rangle/\langle u'w'\rangle \approx 1.2$ (Ref. 8). This gives $b \approx 0.12$ in agreement with the value of $b = 0.125$ used in previous numerical studies.[5,6]

The values of the ratios of the diffusion scales to the macroscale, Λ_2/Λ and Λ_3/Λ, and the ratio of the macroscale to a characteristic length of the flow are chosen on the basis of a computer fit to freejet data. The accuracy of neither the model nor the data are sufficient to determine both Λ_2 and Λ_3 independently. For our purposes here, we will assume $\Lambda_3 = -\Lambda_2$ rather than the assumption $\Lambda_3 = \Lambda_2$ used in Ref. 5. The present assumption has the advantage of making the combined turbulent diffusion terms somewhat simpler. In fact, this permits $\langle u'u'\rangle$ to be equal to $\langle v'v'\rangle$, an equality which is fairly consistent with the available experimental data. Although Chevray's data do show some variation with radius of these two components, it is not consistent enough to warrant a variation between the two components in the model.§

The characteristic length chosen to ratio to the macroscale is the radius $\hat{r}$ at which q falls to one half its maximum value. It

§ A reviewer has pointed out that Y. H. Oh (Ph.D. thesis, 1970, The Catholic University of America) used Donaldson's original equations with $\Lambda_3 = 0$ to predict Chevray's results.

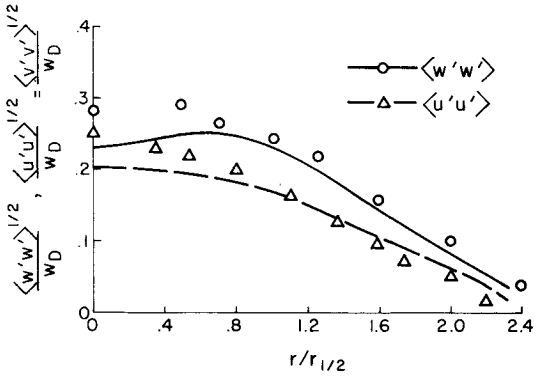

Fig. 2 Velocity fluctuations in a freejet as a function of radius for the same conditions as Fig. 1.

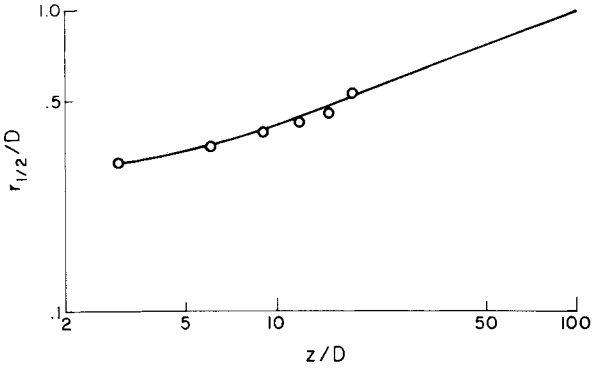

Fig. 4 Wake spread measured by the radius at which the departure of the mean velocity from the freestream velocity reaches one half its maximum value. ○ Chevray's observations; —— model predictions.

might seem more natural to take the radius at which the mean velocity difference between its maximum value and the freestream value falls to one half its maximum value ($r_{1/2}$). But this length turns out to be a somewhat erratic measure for wakes with near zero net momentum, as will be demonstrated later.

Comparisons between model predictions and experimental data for a self-preserved freejet[9] are given in Figs. 1 and 2. The results are sensitive to variations in $\Lambda/\hat{r}$ and b, and relatively insensitive to variations of Λ_2/Λ (Ref. 10). These jet results have been obtained by starting with some assumed nonself-similar velocity and turbulence distributions and letting the jet develop until self-similar distributions are obtained.

A somewhat better match for the energy components would occur for $\Lambda = 0.22\hat{r}$, but a better match for the shear stress distribution would occur for $\Lambda = 0.18\hat{r}$. The value chosen was a compromise of $\Lambda = 0.2\hat{r}$.

Both the shear stress and the energy could be matched if the model for the $\langle p'\,\partial u_i'/\partial x_j\rangle$ terms in Eq. (3) incorporates a term proportional to the mean strain, i.e., if we take

$$\left\langle p'\left(\frac{\partial u_i'}{\partial x_j}+\frac{\partial u_j'}{\partial x_i}\right)\right\rangle = -\frac{q}{\Lambda}\left(\langle u_i' u_j'\rangle - \delta_{ij}\frac{q^2}{3}\right) + \gamma q^2\left(\frac{\partial \bar{u}_i}{\partial x_j}+\frac{\partial \bar{u}_j}{\partial x_i}\right) \qquad (14)$$

Crow[11] has shown for small scale linearized turbulence that γ should have a value of $\frac{1}{5}$. However, this is too large for the self-preserved jet since it would completely override the production terms. A reasonably good fit to the jet can be obtained by taking $\gamma = 0.05$, with $\Lambda = 0.24\hat{r}$ and b increased to 0.15.

To obtain a model that is reasonably valid for a wide group of flows, it is probably best not to try to fine tune it to any one particular special flow. For this reason, plus the fact that it would require a change in b, γ has been set equal to zero in the current model. Mellor and Herring[4] also report that the uncertainty in γ is comparable to its mean value.

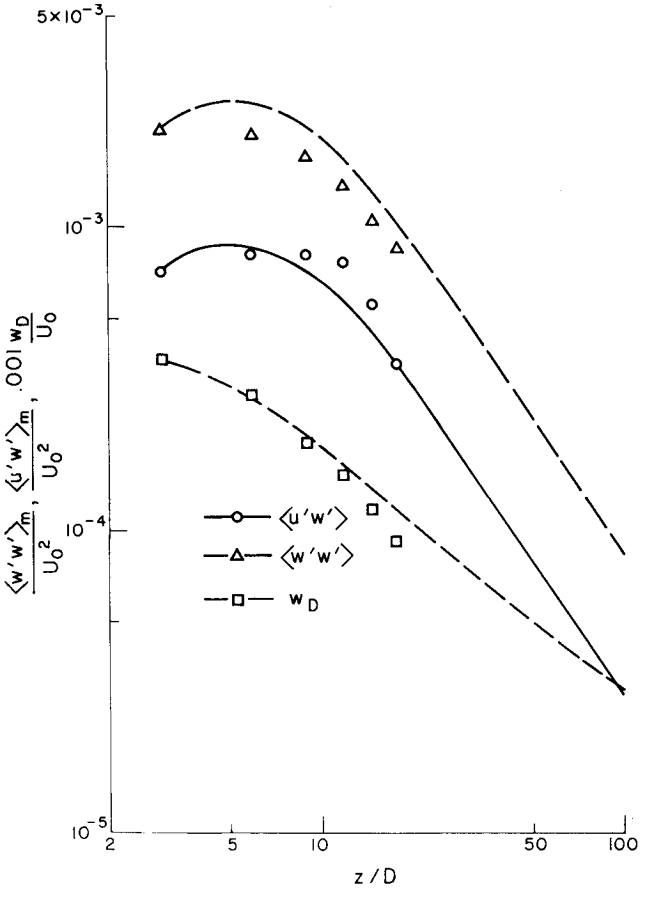

Fig. 3 Mean velocity defect and maximum value of second-order velocity fluctuations as a function of distance downstream from the body. □, △, ○ Chevray's observations; — — model predictions.

Comparison with Chevray's Wake Data

The capabilities of the program to predict the development of a wake was tested by matching the distributions of $\langle u'w'\rangle$, $\langle v'v'\rangle$, $\langle u'u'\rangle$, $\langle w'w'\rangle$ and $\bar{w}$ as observed by Chevray[2] at one axial station and then comparing the program predictions for the wake development with the actual observed development. Chevray measured the mean turbulent characteristics at several axial stations in a wake behind a six-to-one spheroid at a Reynolds number, based on freestream velocity and body length, of 2.75×10^6. His observations at an axial station three diameters downstream of the stern of the body were chosen as initial conditions for the model computations. This should be far enough downstream that the model's assumption of negligible axial pressure gradient be valid, and it permits the comparison of model results with observations at five axial locations further downstream.

The decay of the maximum velocity defect, w_D; the maximum shear stress, $\langle u'w'\rangle_m$; and the maximum axial velocity fluctuation, $\langle w'w'\rangle_m$; are given in Fig. 3. The model predictions for w_D are close to the observations. The model predicts an initial buildup in shear stress before it begins to decay which differs at most by 20% from the experimental observations. The largest discrepancy is in the decay of $\langle w'w'\rangle_m$. The model predicts an increase of 35% over the initial value at $z/D = 3$ which the observations do not show.

The wake spread as measured by the radius for which $|\bar{w} - U_o|$ is equal to half of its maximum value is given in Fig. 4. The agreement again is good. Although Chevray fits a one third power law growth rate to his data at $z/D = 18$, the model indicates

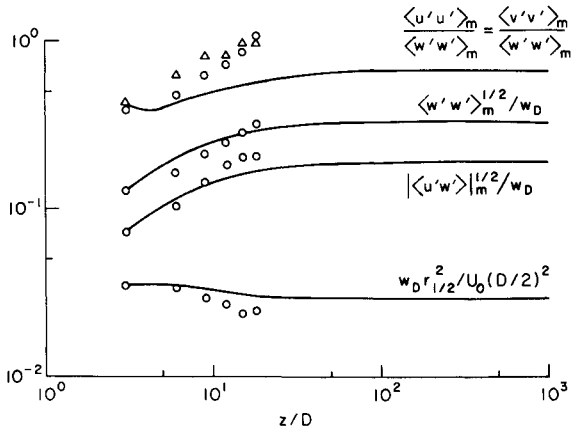

Fig. 5 Some normalized turbulent characteristics as a function of distance, showing the approach to self-similar, constant values. ○, △ Chevray's observations; —— model predictions.

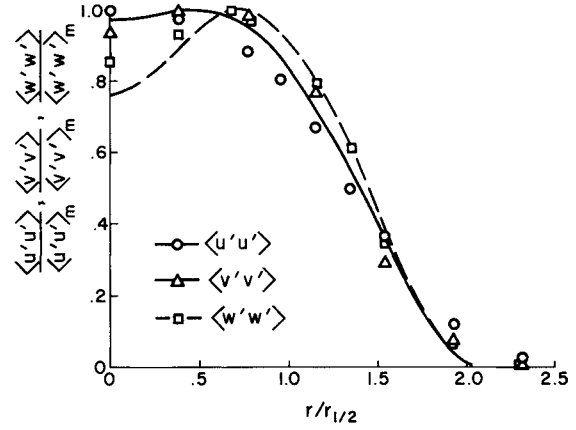

Fig. 7 Radial, tangential and axial velocity fluctuations in a self-similar wake. □, ○, △ Chevray's observations 18 diameters downstream of the body; —— model predictions.

that $z/D \approx 100$ is required for the wake to reach its asymptotic self-similar growth rates. A more sensitive measure of the approach to similarity is given in Fig. 5 where the ratio of axial turbulent fluctuation to maximum mean velocity is plotted. A constant value of 0.33 is reached at $z/D \approx 50$. This is about twice the distance needed for the product of the center line velocity w_D times the square of the wake radius to reach a constant of 0.029. This is 0.81 times the momentum defect normalized by the reference momentum $\rho\pi(D/2)^2U_o^2$

$$M = \int_0^\infty \frac{\bar{w}}{U_o}\left(\frac{\bar{w}}{U_o} - 1\right)\frac{2r\,dr}{(D/2)^2} = -0.036 \qquad (15)$$

Other characteristics of the self-similar wake are $\langle u'w'\rangle^{1/2}/w_D = 0.19$ and $\langle u'u'\rangle/\langle w'w'\rangle = 0.67$. This last characteristic is in disagreement with the experiment which indicates that the turbulent fluctuations are approaching an isotropic state. It is difficult to see how the apparent observations can be correct since in the self-similar state, there is a continual production of the $\langle w'w'\rangle$ component of turbulence forcing the turbulence to be nonisotropic.

The self-similar profiles obtained by the model for $z/D \geqq 100$ are compared in Figs. 6 and 7 with the distributions measured by Chevray at his farthest downstream station. For these distributions both the model results and the data have been normalized by the maximum value of the variable at that axial station. The comparisons are quite good even though the experimental wake has not quite reached its asymptotic, completely self-similar state.

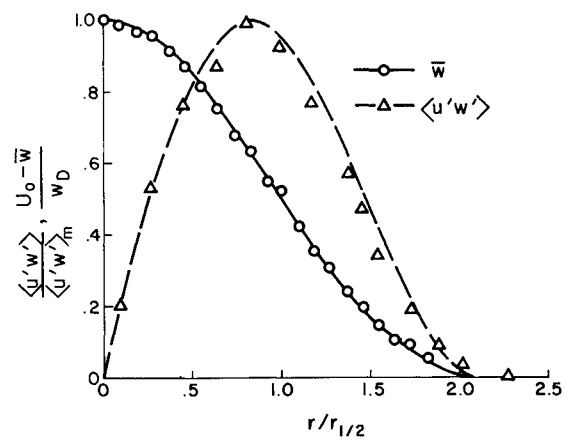

Fig. 6 Normalized mean velocity and shear stress distributions of a self-similar, axisymmetric wake as a function of normalized radius. ○, △ Chevray's observations 18 diameters downstream of the body; —— model predictions.

Comparison with Naudascher's Wake Data

When the integral of the momentum flux in the far wake is zero, the rate of the turbulence decay may be quite different from that for a finite momentum wake. Naudascher[1] has reported on the most detailed measurements of a wake approximating this case that is available in the literature. A self-propelled body was simulated by a stationary disk mounted on the end of a tube in a wind tunnel. Flow was provided through the tube to yield a jet with just sufficient thrust to reduce to zero the net force on the tube-disk arrangement to within 0.5% of the reference momentum $\rho\pi(D/2)^2U_o^2$. The Reynolds number based on freestream velocity and disk diameter was 5.5×10^4.

Naudascher's observed radial distributions at an axial station seven disk diameters downstream of the disk were chosen as

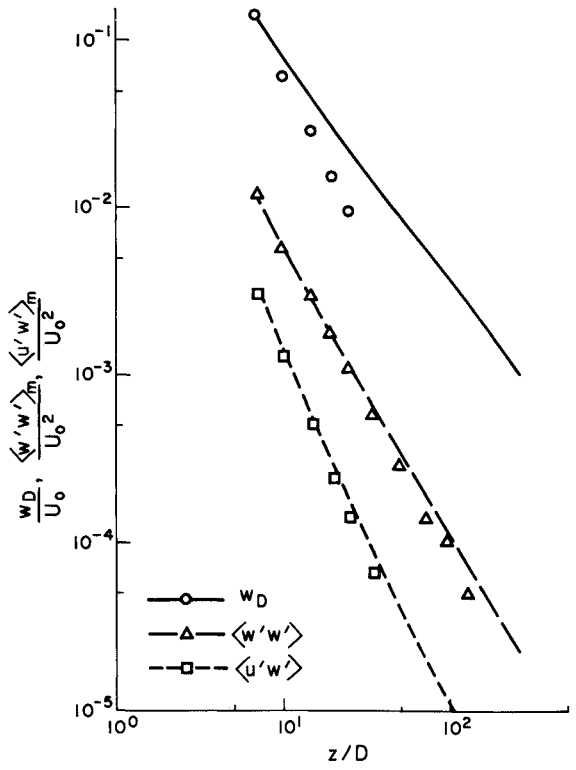

Fig. 8 Maximum values of mean velocity departure from freestream, axial velocity fluctuations, and shear stress as a function of distance downstream of a self-propelled body. ○, □, △ Naudascher's observations; —— model predictions.

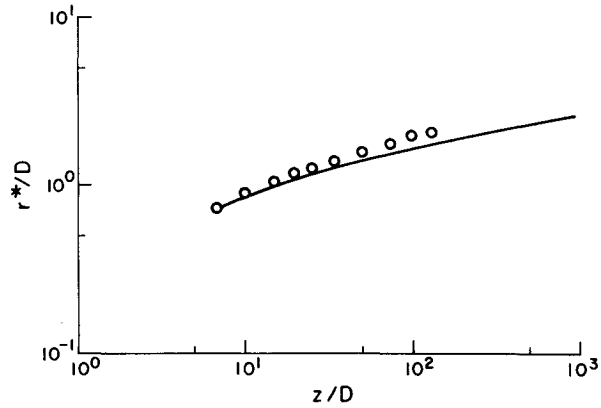

Fig. 9 Wake spread measured by the radius r^* at which $\langle w'w' \rangle^{1/2}$ reaches one half its maximum value. ○ Naudascher's observations; —— model predictions.

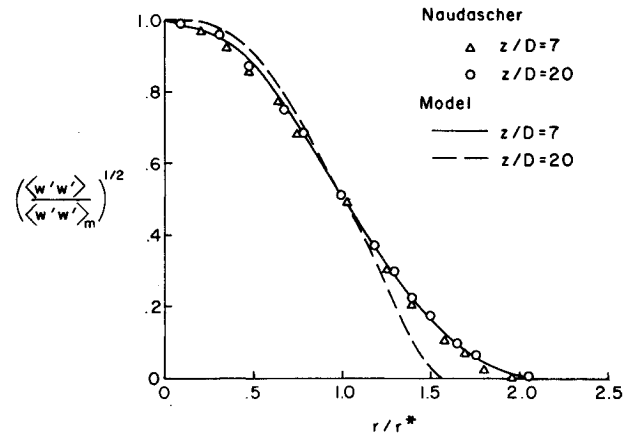

Fig. 11 Normalized axial velocity fluctuation distribution at two axial stations in the wake of a self-propelled body.

initial conditions for the model computations. This is somewhat farther downstream than the previous starting point because of the apparently large pressure gradients in the near wake. Figure 8 is a plot of the maximum velocity difference, the maximum axial velocity fluctuations, and the maximum shear stress as a function of distance downstream. The agreement between model and observations is not too good for the mean velocity. The predicted decay rate is about 17% slower than that observed. On the other hand, the decay rate for $\langle w'w' \rangle_m$ is in good agreement with the data. The maximum shear stress decay is also in very close agreement with the observed decay, while the wake spread as measured by the radius at which the axial turbulence intensity reaches half of its maximum value is observed to grow at a slightly faster rate than that predicted by the model (Fig. 9).

The mean velocity profile normalized by its maximum departure from freestream is given in Fig. 10 at two axial stations, the initial profile used for the computations and the profile at $z/D = 20$. The initial profile for the model differs somewhat from the experimental observations at $z/D = 7$. An average curve representing measurements at six different stations was used for the input profile. Little change in this normalized profile is observed at $z/D = 20$.

Figure 11 gives the radial distribution of the axial velocity fluctuations. Here there is a noticeable shift in the model profile at $z/D = 20$. A shift in the tail of the distribution also occurs in the shear stress distribution in Fig. 12. Taken together, Figs. 10–12 show that the model does a reasonable job in maintaining the appropriate normalized distributions for this flow for which there is no precise similarity.

The largest discrepancy between the model results and experimental observations is that of the velocity defect decay shown in Fig. 8. The fact that the shear stress axial and radial distributions are in good agreement suggest some possible inconsistency within the data. In analyzing the data, the possible contributions to the momentum balance which we have left out, $(1/\rho)\partial p/\partial z + \partial \langle w'w' \rangle/\partial z$ contribute only about 5% and so can not explain the discrepancy. If the normalized velocity and the shear stress distributions are to be self-similar then $\approx 20\%$ steeper slope for the shear stress distribution at $r = 0$, $[\partial \langle u'w' \rangle/\partial r]_{r=0}$, is required to make the data internally self-consistent. For the model to predict a steeper slope at $r = 0$ would appear to require the scale model to have a radial variation with Λ increasing as r increases.

The far wake development depends strongly on how nearly zero the net momentum is. Any finite momentum will eventually influence the far wake. The smaller the momentum the farther downstream this influence is delayed. This is illustrated in Fig. 13 where the model results for different values of momentum are given. The top velocity-defect decay curve corresponds to the Chevray run which asymptotically reaches the classical two-thirds power-law decay. The other three curves are for three slight variations of the Naudascher input data. The velocity defect distribution is altered to change the net value of M in Eq. (12). Since the contributions of the plus and minus portions of

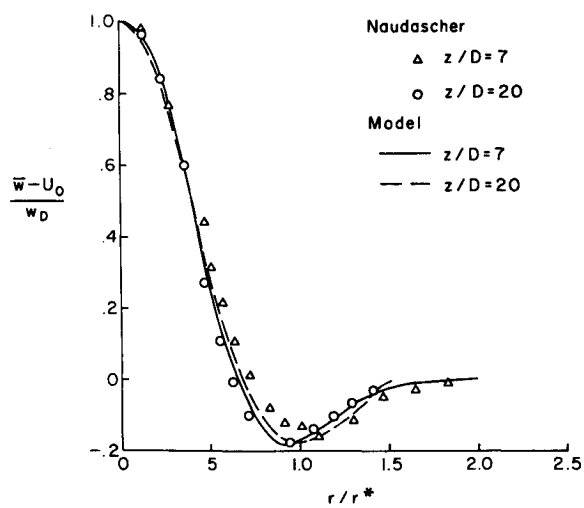

Fig. 10 Normalized mean velocity distribution at two axial stations in the wake of a self-propelled body.

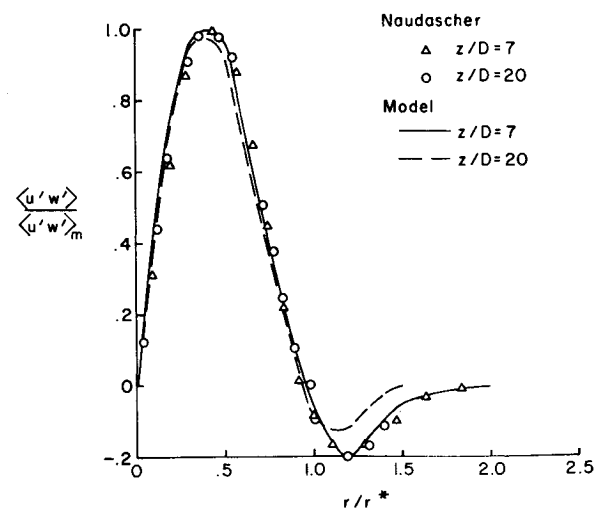

Fig. 12 Normalized shear stress distribution at two axial stations in the wake of a self-propelled body.

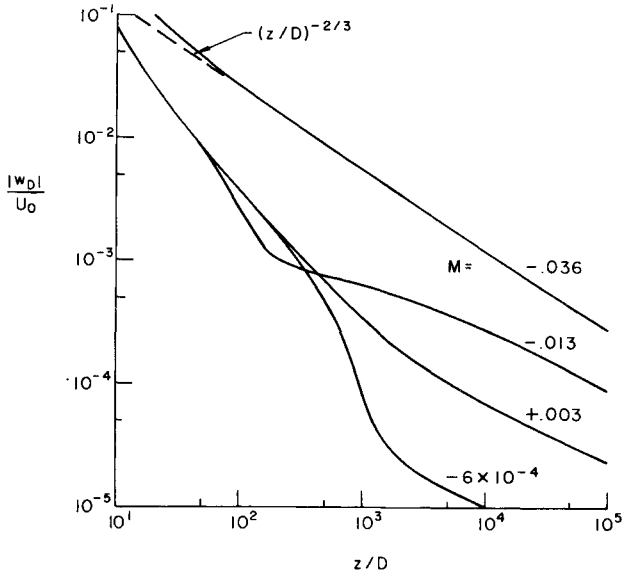

Fig. 13 Maximum mean velocity departure from freestream as a function of downstream distance and net momentum defect. $M = -0.036$ for Chevray's conditions; $|M| < 0.005$ for Naudascher's conditions.

the curve, Fig. 10, very nearly balance, small variations are sufficient to obtain the three values of M used. The velocity defect decay is the same for all three up to $z/D \approx 50$. Then the case for the largest value of M departs markedly from the other two. The two curves for $M = +0.003$ and -6×10^{-4} coincide up to $z/D \approx 200$, at which point the curve with the negative momentum begins to decay much faster.

Naudascher only claims that $|M| < 0.005$. (The characteristics given in Figs. 8–12 are for the lowest value of $M = -6\times10^{-4}$.) These three values of M (Fig. 13) produce no change in the decay rate of $\langle w'w'\rangle^{1/2}$ for $x/D < 10^4$. In fact, the effect of flow Reynolds number appears before the effect of M. For a Reynolds number, based on r^* at $z/D = 7$ and freestream velocity, of 4×10^4, which corresponds closely to Naudascher's reported value, viscosity increases the decay rate of turbulence for $z/D \geqq 10^3$. When the Reynolds number is increased by two orders of magnitude the turbulence fluctuation decays at a rate of $(z/D)^{-3/4}$ for $10^2 < z/D < 10^5$. This is the same decay rate as that reported by Merritt[12] for a wake behind an oscillating grid simulating a self-propelled body.

A wake with near zero net momentum appears to have a type of locally similar decay with $q \sim z^{-3/4}$ with the velocity defect decaying at a much faster rate. This continues until $w_D {r_{1/2}}^2 = O(M)$, at which time the w_D decay flattens out and the wake transitions to the true self-similar profiles given in Figs. 6 and 7. For the case with $M = -0.013$, the maximum negative value of w_D is almost equal to the centerline positive value at $z/D = 100$, where from Fig. 13 the sharpest drop in w_D is occurring. By approximately $z/D = 200$, the positive portion of w_D has completely disappeared and it gradually approaches the profile of Fig. 6, providing the Reynolds number of the turbulence remains high enough to allow the microscale governing the dissipation to be proportional to $(\nu\Lambda/q)^{1/2}$ [see Eq. (12)].

As long as the Reynolds number is sufficiently large the bottom three curves in Fig. 13 would approach the $z^{-2/3}$ asymptote far downstream. Far enough downstream, differences in momentum would have the same effect as shifts in the initial x position.

It is clear that the radius at which w_D reaches one half its maximum value would not be a good characteristic length for the flow in the region where the velocity profile is changing drastically. This was the prime reason for taking Λ proportional to the radius at which q reaches one half its maximum value.

Conclusions

The comparisons made in the preceding figures show that we have developed a computer model that is capable of reasonably accurate predictions of the decay of an incompressible turbulent wake as a function of momentum and initial turbulent distributions. Predictions of w_D, $\langle u'w'\rangle$, $\langle w'w'\rangle$, $\langle u'u'\rangle$, and $\langle v'v'\rangle$ are made as a function of distance z, or equivalently time t, and radial position. Wakes with near zero net momentum flux are shown to exhibit a type of local similarity for some distance downstream of the body before they transition to the truly self-similar state characterized by their finite momentum flux.

References

[1] Naudascher, E., "Flow in the Wake of Self-Propelled Bodies and Related Sources of Turbulence," *Journal of Fluid Mechanics*, Vol. 22, 1965, pp. 625–656.

[2] Chevray, R., "The Turbulent Wake of a Body of Revolution," *Journal of Basic Engineering*, Vol. 90, Ser. D, 1968, pp. 275–284.

[3] Bradshaw, P., "The Understanding and Prediction of Turbulent Flow," *Aeronautical Journal*, Vol. 16, July 1972, pp. 403–418.

[4] Mellor, G. L. and Herring, H. J., "A Survey of Mean Turbulent Field Closure Models," *AIAA Journal*, Vol. 11, No. 5, May 1973, pp. 590–599.

[5] Donaldson, C. duP., "Calculation of Turbulent Shear Flows for Atmospheric and Vortex Motions," *AIAA Journal*, Vol. 10, No. 1, Jan. 1972, pp. 4–12.

[6] Donaldson, C. duP., "Construction of a Dynamic Model of the Production of Atmospheric Turbulence and the Dispersal of Atmospheric Pollutants," *Workshop on Micrometeorology*, edited by D. A. Haugen, American Meteorological Society, Boston, Mass., 1973, pp. 313–390.

[7] Bradshaw, P., Ferriss, D. H., and Atwell, N. P., "Calculations of Boundary Layer Development Using the Turbulent Energy Equation," *Journal of Fluid Mechanics*, Vol. 28, March 1967, pp. 593–616.

[8] Cramer, H. E., "Turbulent Transfer Processes for Quasi-Homogeneous Flows within the Atmospheric Surface Layer," *Physics of Fluids*, Vol. 10, 1967, Suppl. S240–S246.

[9] Wygnanski, I. and Fiedler, H., "Some Measurements in the Self-Preserving Jet," *Journal of Fluid Mechanics*, Vol. 38, March 1969, pp. 577–612.

[10] Lewellen, W. S., Teske, M., and Donaldson, C. duP., "Application of Turbulence Model Equations to Axisymmetric Wakes," Rept. 191, Feb. 1973, Aeronautical Research Associates of Princeton, Princeton, N.J.

[11] Crow, S. C., "Viscoelastic Properties of Fine-Grained Incompressible Turbulence," *Journal of Fluid Mechanics*, Vol. 33, Jan. 1968, pp. 1–20.

[12] Merritt, G. E., "Wake Growth and Collapse in Stratified Flow," AIAA Paper 73-108, Washington, D.C., 1973.